We are IntechOpen, the world's leading publisher of Open Access books Built by scientists, for scientists

4,800
Open access books available

122,000
International authors and editors

135M
Downloads

Our authors are among the

154
Countries delivered to

TOP 1%
most cited scientists

12.2%
Contributors from top 500 universities

CLARIVATE ANALYTICS BOOK CITATION INDEX INDEXED

WEB OF SCIENCE™

Selection of our books indexed in the Book Citation Index in Web of Science™ Core Collection (BKCI)

Interested in publishing with us?
Contact book.department@intechopen.com

Numbers displayed above are based on latest data collected.
For more information visit www.intechopen.com

27

Binding of Protein-Functionalized Entities onto Synthetic Vesicles

Federica De Persiis[1], Ramon Pons[2], Carlotta Pucci[1], Franco Tardani[1] and Camillo La Mesa[1,3]
[1]*Dept. of Chemistry, La Sapienza University, Rome, Italy*
[2]*Institut de Química Avançada de Catalunya, IQAC-CSIC*
[3]*SOFT-INFM-CNR Research Centre, La Sapienza University, Rome*
[1,3]*Italy*
[2]*Spain*

1. Introduction

Mono-disperse silica nano-particles with pending functional acid groups lying on their surface were reacted with coupling agents and, then, with lysozyme, to get protein-functionalized entities. The synthetic procedure reported therein gives tiny amounts of protein functionalized sites; surface coverage by the protein is, thus, moderate. The amount of covalently bound lysozyme was estimated from *UV*-vis methods and resulted to be about <5> molecules per nano-particle. Electro-phoretic mobility experiments indicate the occurrence of significant variations in surface charge density of functionalized nano-particles compared to the original ones and ensure a significant binding efficiency onto reconstructed, or synthetic, vesicles.

Protein-functionalized nano-particles form clusters and are readily re-dispersed by application of shear methods. Thereafter, they remain in disperse form for long times. According to *DLS*, protein-functionalized nano-particles interact with either cationic or cat-anionic synthetic vesicles. Care was made to ensure that nano-particles and vesicles have comparable sizes. The above procedure ensures to determine the fate of the reactive pathways by *DLS*. At room temperature and moderate ionic strength, the binding of protein-functionalized entities onto the aforementioned vesicles is completed in about one hour. The nano-particle vesicle complexes precipitate as fine powders, or form large floating objects, depending on vesicle size, relative concentrations of protein-functionalized particles and their net charge (which is related to the *pH* of the dispersing medium).

The binding efficiency for the above processes is controlled by the overlapping of repulsive and attractive interactions between particles and vesicles. The kinetic pathways relative to the interactions between vesicles and nano-particles were investigated, and significant differences were met in the two cases. Some technological implications of the above systems are preliminarily discussed. For instance, it is stated that interactions between nano-particles and vesicles mimic those occurring between cells and solid particles, or viral vectors, located in the medium surrounding vesicles.

Graphical Abstract

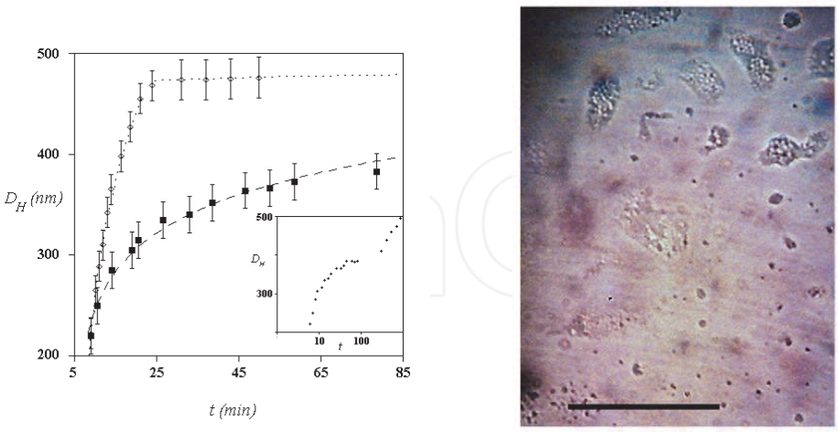

Left, Dependence of the size of nano-particle/vesicle clusters on reaction time, inferred by DLS methods.
Right, Clusters of vesicles and protein-functionalized nano-particles obtained by mixing DDAB vesicles and nano-particles in number ratio 300/1. Images were visualized through a Zeiss optical microscope using normal light. The bar size in the left bottom of the figure is 100 mm large.

Nanotechnologies deal with the synthesis, the characterization, the production and the application of objects and devices operating at the nano-scale level [1]. As a consequence of substantial interest in this field, many scientific journals and books are progressively addressing attention to nano-technologically oriented items. The same holds for the number of patents relative to these subjects. This is because the demand on the possible applications of the above materials is drastically increasing in the last few years. Practical applications are manifold and find use in electronics, in the preparation of magnetic devices, in chemistry (mostly in the field of heterogeneous catalysis), but also in biotechnology and biomedicine.
Materials at the nano-scale are widely different each from the other in chemical composition, size and surface functionalities. Particles properties depend on the preparation procedures and can be tailored accordingly. Nano-particles can be made of metals, oxides, polymers and/or a combination thereof. Properly functionalized particles, such as quantum dots, spheres, disks, filaments, tubes and composite objects (all in the nano-meter size range) find substantial application in the aforementioned fields.
In this contribution, we report on silica nano-particles, onto which a protein, lysozyme, was covalently bound [2,3]. The synthetic part of the work is reported below. The same holds for the characterization of the resulting hybrid composites. A substantial amount of work was needed to ensure the required performances to nano-particles, which were tailored in terms of state of the dispersion, size, stability and net charge. Obviously, the above effects are strongly interrelated each other. The reasons for using protein-functionalized entities arise by the need to have objects at the nano-scale level, characterized by a significant number of bound proteins. Apart from intrinsic interest towards the structural properties of hybrid nano-composites, the advantages of protein-functionalized particles are manifold compared to other bio-medical formulations, since:

i. the surface area of the resulting nano-composites can be properly controlled,
ii. the number of covalently bound proteins can be modulated accordingly, and,
iii. the conformation of proteins adsorbed therein can be somehow predicted [4].

Silica was used as an anchoring site because of its good bio-compatibility, which is substantially higher compared to polymer-based nano-particles. It is particularly useful since blood and other bio-fluids contain markers adsorbing on the surface of hydrophobic carriers, and indicating to *RES* (the *Reticulum Endothelial System*) the urgency to remove them from the target tissue [5]. Conversely, silica nano-particles (*NP*s) are of friendly use with biological tissues. As most inorganic oxides, SiO_2 is strongly hydrophilic in character. Such property increases its compatibility and ensures a safe circulation in bio-fluids. In addition, it is possible to anchor efficiently proteins or other biologically active substances onto mono-dispersed silica.

Lysozyme was chosen to test the covalent binding efficiency onto nano-particles because of its ubiquitary nature. In the following, we report on anchoring efficiency and do not explicitly account for the effect that *pH*, salts or other substances have on the fate of protein-functionalized *NP*s in biological matrices. The present communication only focuses on the synthesis and characterization of such materials.

In the second part of this contribution the interactions between protein-functionalized silica *NP*s and synthetic vesicles were experienced. The synthetic vesicles dealt with in this contribution are also relatively mono-dispersed, thermodynamically, or kinetically, stable and are characterized, in some cases, by a bi-layer structure [6]. Hence, they can be considered the synthetic analogues of cell membranes. Were the interactions between vesicles and *NP*s effective, the possibility of surface adhesion, or encapsulation, can be realized. Perspectives of these complex systems as composite drug-delivery carriers are, thus, at hand.

We choose different vesicle-forming materials based on a synthetic double-chain surfactant and mixtures of different surface active species. The performances of the former class, based on quaternary ammonium salts, were extensively characterized by Barenholz and coworkers [7,8]. Such species, however, are of questionable utility for biomedical applications, since most quaternary ammonium salts have strong anti-bacterial character. In addition, the vesicles they form are intrinsically meta-stable and progressively coagulate into large entities.

Recently, alternatives to the above lipido-mimetic systems were proposed; they rely on systems obtained by mixing oppositely charged surfactants, or lipids, in due amounts. Such mixtures are currently defined by the acronym cat-anionic. These systems came in use since when Kaler and Khan independently characterized some of them [9,10]. In cat-anionic systems the vesicle size and net charge are tuned by modulating the ratio between the two components, provided one of them is in excess. (N.B. If not, the 1/1 mixtures precipitate out.) It is possible, thus, to get negatively or positively charged vesicles. This can be relevant in case vesicles should selectively interact through electrostatic interactions with proteins [11] or *DNA* [12] and form complexes, or lipo-plexes, with the above substances.

In the following we report on the synthetic procedures we have followed, on the optimization required getting stable dispersions of hybrid protein-silica colloids, and on their interactions with vesicles. For reasons to be discussed later, the characterization of the above protein-silica composite material is based on the combination of optical (*UV-vis* or *CD*), dynamic light scattering, *DLS*, and electro-phoretic mobility methods. Some relevant results are briefly reported in the forthcoming sections. Biomedical applications, which are

surely relevant, require dedicated formulation work and need substantial studies on the cyto-toxicity of vesicles, lysozyme-bound *NP*s and of the related adducts. The former systems were previously characterized on this regard by some of us [13], but almost nothing is known on the latter ones.

2. Experimental section

Materials. 3-aminopropyl-(3-oxobutanoic acid)-functionalized silica *NP*s, termed *APOB*, contain significant amounts of carboxylic acids on their surface. They are given from the purveyor (Sigma Aldrich) as 2.5% (w/v) dispersions in dimethylformamide, *DMF*. Their nominal density is 0.927 g ml^{-1} at 25°C [14]. *NP*s were dialyzed against aqueous Borax (50 millimol, pH 8.5) under stirring, sonicated and recovered. The resulting dispersions are relatively stable, since *APOB* nano-particles bear negative charges on their surface.

Hen yolk lysozyme, *LYS*, (Sigma Aldrich) was dialyzed, crystallized, lyophilized and dried over P_2O_5. Its purity was confirmed by ionic conductance, density and viscosity of the corresponding aqueous solutions, at 25.00 °*C* [15,16].

Sodium dodecylsulfate, *SDS*, cetyltrimethylammonium bromide, *CTAB*, and didodecyl-dimethylammonium bromide, *DDAB*, (Sigma Aldrich) were individually dissolved in ethanol and precipitated by addition of cold acetone. The products were vacuum dried at 70°C. Their purity was confirmed by conductometric determination of the critical micellar concentration, *CMC*, at 25.00 °C. *Pluronic F-127* (Sigma Aldrich), a surface active block co-polymer, forming micelles at high temperatures [17], was used as dispersant, when required.

A water soluble carbodiimide, termed *EDAC*, hydroxysuccynimide, *NHS*, triethylamine, $N(Et)_3$, and glycine, (Sigma Aldrich), were used as such.

3. Materials preparation

LYS-ABOP nano-particles. 20 mg of *APOB* in 50 millimolar kg^{-1} (*mmol*) aqueous Borax were added with 13.0 mg *EDAC*, 10.0 mg *NHS* and7.27 mg $N(Et)_3$, at 25°C [7], and homogenized upon stirring. 44.13 mg solid *LYS* was added and the reaction proceeded for 5 hours, at 40°C. The reaction between *ABOP* and *LYS* is concomitant to an increase in opalescence of the dispersions, due to both a decreased surface charge density (because of the reaction of *COOH* groups with *EDAC)*, and to protein covalent binding. The final dispersion was centrifuged at 12000 rpm for 10 minutes, at 4°C. Thereafter, 10 mmol glycine was added, to quench un-reacted groups that were eventually bound onto *NP*s. The latter procedure significantly reduces the dispersion turbidity. A summary of the whole synthetic procedure, in four stages, is sketched in *Scheme 1*, where are indicated the different preparation steps.

Prolonged sonication, dialysis, with pH and/or ionic strength adjustment significantly tailors the average size of *NP*s and reduces their size. Substantial characterization is required to ensure the attainment of equilibrium conditions, since the size of particles increases with aging, *Figure 1*. The dispersions were extensively dialyzed against the buffer, until no more lysozime, *EDAC* and/or *NHS* was determined in the supernatant. To avoid the occurrence of clusters, the dispersions must be sheared [18] or forced to flow in tilted long syringe steel needles [19], as indicated in *Figure 2A*.

Synthesis of Lys-ABOP nano-particles: a reactive scheme

Step 1

P-NH-R-COOH (*in DMF*) —*dialysis*, *Borax 50 mmol*, *pH 8.5*→ *P-NH-R-COOH* (*in Borax buffer*)

Step 2

P-NH-R-COOH (*in Borax buffer*) —*+ EDAC + N-suc + N(Et)3*, *Borax 50 mmol, 25° C*→ *Active*

Step 3

Active + Lyso —*10 mmol Glycine*, *Borax 50 mmol*→ *Lys-ABOP nano-particles*

Step 4

Dialisys + pH conditioning + ionic strength control + centrifugation

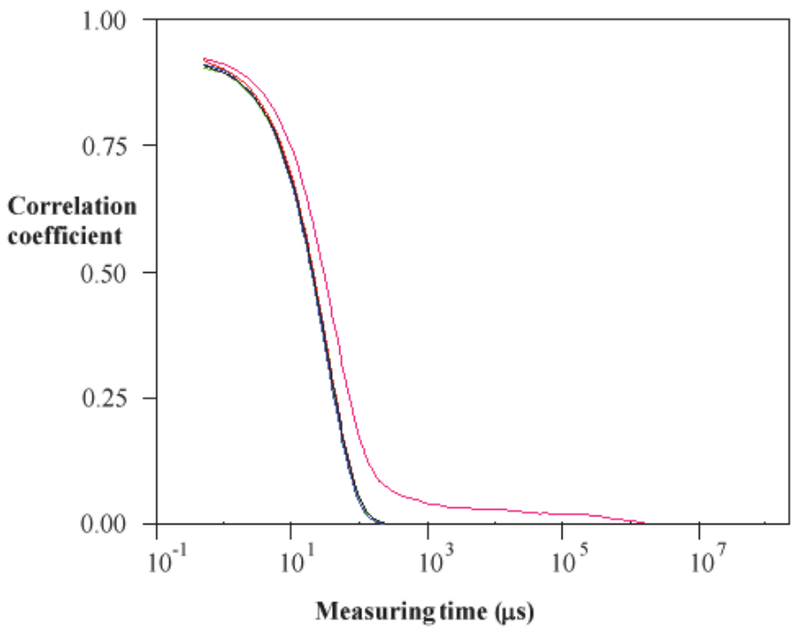

Fig. 1. Plots of the correlation coefficient (in arbitrary units) versus the measuring time, in µs, for a 0.20 wt/vol % dispersion of Lysozyme-ABOP nano-particles (in 50 mmol Borax buffer, pH 8.5, at 25°C) one day after preparation, in blue, one week, in orange, and one month, in cyan.

When particles are subjected to shear forces during flow, large aggregates break down. This procedure decreases the size of *LYS/ABOP NP*s, *Figure 2B*.
Cat-anionic vesicles were prepared by mixing 6.00 *mmol* aqueous *SDS* with 6.00 *mmol CTAB*, in due proportions. Optimal sizes and surface charge density occur when the mole ratio between *SDS* and *CTAB* is in the range 1.5-2.5. The dispersions are milky, because multi-lamellar, and size-poly-disperse, vesicles occur. It was formerly observed, however, that heating them to temperatures close to 50°C reduces the average size of multi-lamellar vesicles, with formation of truly bi-layered entities [20]. Thereafter, vesicles remain in such state for over two months, even when they are kept at room temperature.

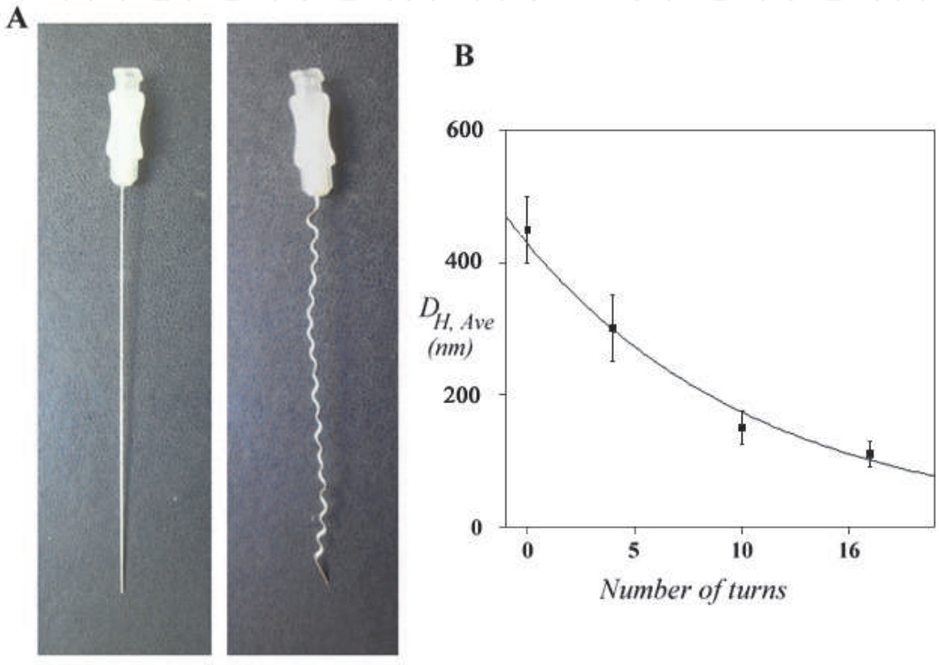

Fig. 2. A; View of iron steel needles, tilted to increase the number of turns. B; Reduction in size of 0.12 w/v % LYS-ABOP nano-particles obtained by coupling (and dispersed in 50 mmol Borax, pH 8.5, at 25°C) when forced to flow in tilted needles. Data are reported as average particles size (nm) versus number of turns in the needle. Each sample was forced to flow in the needles for 50 times.

DDAB vesicles are multi-layered entities and their properties were tailored by extrusion and/or thermal cycling. Both vesicular dispersions were thermally equilibrated at 25.0°C soon after the preparation procedures and controlled over a long-time scale. Temperatures lower than 20°C were avoided, since they imply partial surfactant precipitation in the *SDS-CTAB* system.

4. Methods

Dynamic Light Scattering. A Zeta Nanosizer unit, Malvern, performed measurements at 632.8 nm, in back scattering mode (*BSM*), at 173°. This configuration minimizes multiple scattering and allows measuring poly-disperse systems. The unit performances were checked by standard procedures [21]. Thermal equilibrium was controlled by a Peltier unit, at

25.0°C. The dispersions were passed through 0.80 μm Millipore filters and equilibrated at 25.0° or 37.0°C for some minutes. Correlation fits of the light scattering intensity were elaborated by *CONTIN* algorithms [22]. The auto-correlation decay function, $g_1(\tau)$, determined the self-diffusion coefficient, and the hydrodynamic radii were evaluated by the Stokes-Einstein equation ($D_{app} = K_B T / 6\pi\eta R_H$). The uncertainty on vesicles sizes is to 10-20 nm, depending on their size.

ζ-potential measurements. ζ-potential methods determined the surface charge density, σ, of particles moving under the effect of an applied electric field, $\bar{E}$ [23]. A laser-Doppler utility performed measurements, at 25.0°C, in cells equipped with gold electrodes. The scattered light passing in the medium, subjected to the action of $\bar{E}$, shifts in frequency compared to unperturbed conditions. Data manipulation of the signal gives the ζ-potential ($\zeta = 4\pi\sigma\tau / \varepsilon^{\circ}$, where τ the double layer thickness and ε° the static dielectric constant of the medium). The uncertainty on ζ-potentials is 0.5-1.0 mV. Data are reported in *Figure 3*.

Ionic Conductivity. The electrical conductance, κ *(S cm-1)*, was determined by a Wayne-Kerr impedance bridge, at 1 *KHz*, using a Daggett-Krauss cell thermostated to 25.00±0.01°C.

CD. Measurements were run on a Jasco J-715 unit, working with 1 nm resolution. 0.100 cm quartz cells were used. Spectra are the average of three independent runs in the 190-300 nm range. Signals due to native *LYS*, at 208 and 222 nm, respectively, were determined.

UV-Vis Light Absorbance. Light absorption spectra, *A*, were recorded in the range 190-300 nm by a Jasco V-570 unit, at 25.0±0.1 °C; the cell path length was 0.100 cm.

Microscopy. Optical microscopy, in normal or polarized light, was performed through a Zeiss optical microscope.

Density. The particles density was determined by a DMA-60 Anton Paar vibrating densimeter, and thermally controlled by a water circulation bath working at 25.00 ± 0.01 °C.

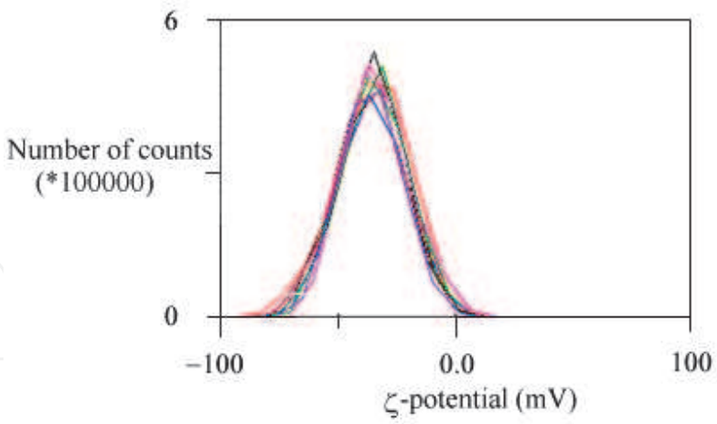

Fig. 3. Plot of ζ-potential values for different dispersions of nominal concentration in LYS-ABOP nano-particles equal to 0.12 w/v %. Measurements were run in 50 mmol Borax, at 25.0°C. Data are reported as number of counts (*10^5) vs. measured ζ-potential value.

5. Results and discussion

Nano-particles characterization. Nano-particles made of *LYS* and *APOB* (termed as *LYS-ABOP*) were characterized by *DLS*, *CD*, *UV-vis* and ζ-potential methods. A substantial amount of

work was required to stabilize the resulting dispersions, because of their tendency to agglomerate and/or phase separate. The optimal conditions for an effective stabilization (i.e. stirring, temperature, *pH* and/or ionic strength) were determined. The surface charge density, σ, plays a pivotal role in the stability of these dispersions and depends on the medium ionic strength. In buffers with 50 mmol Borax and 10 mmol *NaCl* the dispersions remain stable for about two weeks; usually, they were used one day after preparation. Care was taken to get macroscopic homogeneity and to avoid the presence of clusters or sediments.

In the characterization by *DLS*, a proper selection of the elaborating functions, taking into account the particles sizes and poly-dispersity, was necessary. The cumulant method was applied and the scattering equation, $g_1(t)$, was expressed as a power-law series, according to the well-known relation

$$\ln g_1(t) = \sum_{n=1}^{\infty} \Gamma_n \frac{(-t)^n}{n!} = -\Gamma_1 t + \frac{1}{2!}\Gamma_2 t^2 - \frac{1}{3!}\Gamma_3 t^3 + \ldots\ldots \quad (1)$$

Eq. (1) gives information on the average value of the distribution function, (that is $\Gamma_1 = \langle\Gamma\rangle = q^2\langle D_{app}\rangle$), and on poly-dispersity index, *PdI* (Γ_2/Γ_1^2). Minor terms are also present.

Even when the particles number is moderate, a prolonged aging of the dispersions must be avoided, since a significant shift of the correlation functions is observed, *Figure 1*. That is, both Γ_1 (related to the particles self-diffusion, D_{app}) and Γ_2 (related to *PdI*) depend on aging. This implies the presence of reactive terms. Data were analyzed accounting for the diffusive contributions pertinent to nano-particles and for the respective reactive terms, respectively. The results are expressed in terms of the relation

$$I_2(t) = \left[|I_1(0)|^2 + |I_1(t)|^2 \right] \quad (2)$$

where $I_2(t)$, $I_1(0)$ and $I_1(t)$ are the scattering intensity at time *t,* the original value at time zero and the reactive part, respectively.

DLS data were interpreted according to Berne and Pecora [24]. Attractive terms, due to particles coagulation, and electrostatic ones, due to the presence of repulsive or attractive forces between colloid entities, are introduced in the time-dependent scattering functions. The relation contains a reactive term, related to the formation of large particles, and is balanced by a flux, in which mobility and diffusive terms are accounted for [24]. Accordingly,

$$\left(\frac{\partial c_a}{\partial t}\right) + \nabla \bullet J_a = k_b c_b - k_a c_a \quad (3)$$

where (dc_a/dt) indicates the production, or disappearance, of particles with time. The second term in the right hand side of the equation is expressed as

$$J_a = \mu_a \bar{E} c_a - D_{app,a} \nabla c_a \quad (4)$$

where μ_a is the electro-phoretic mobility of a class of particles, at concentration c_a, under the effect of and applied electric field, $\bar{E}$, and D_{app} is the self diffusion times the concentration gradient, ∇c_a. K_a and K_b are the kinetic constants of reactants, *a*, and products, *b*, respectively.

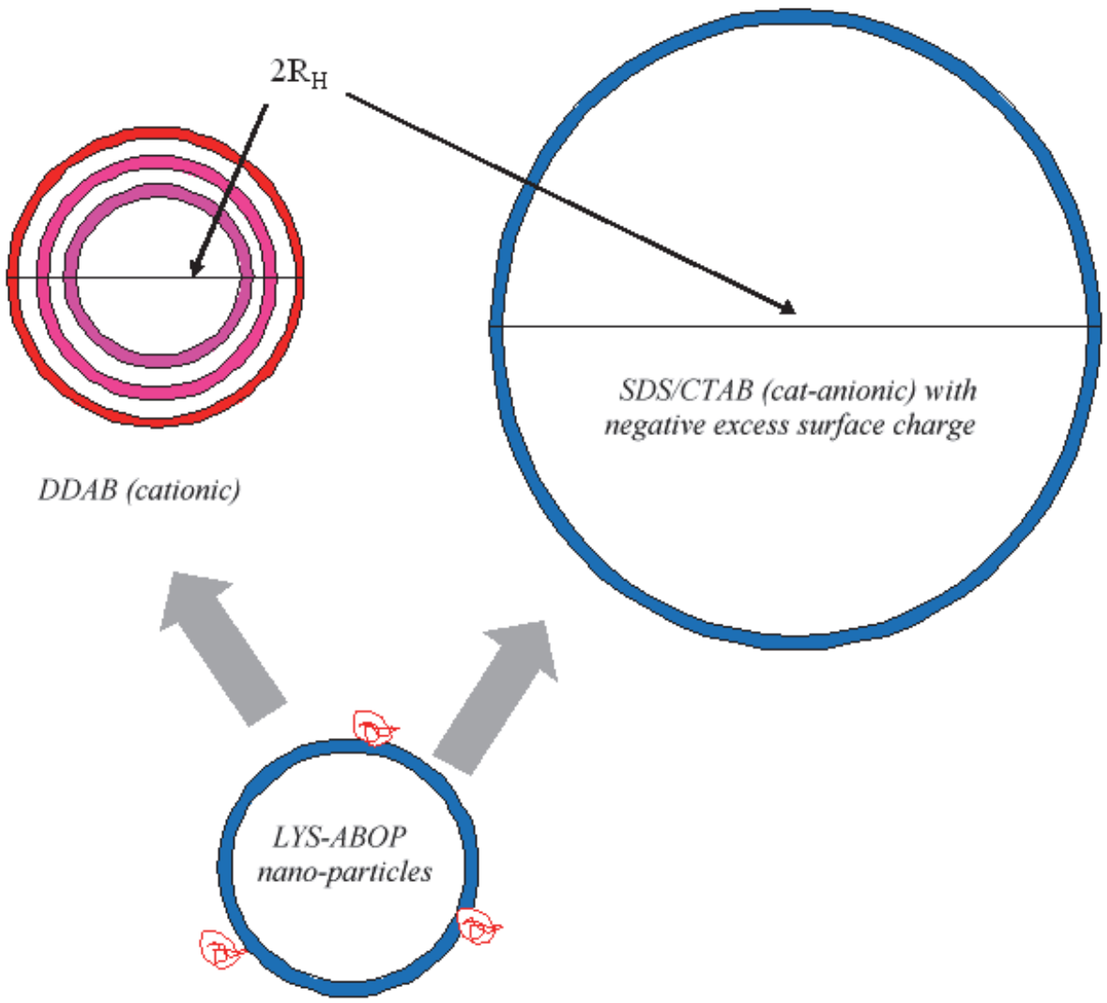

Fig. 4. In the top is reported a schematic representation of vesicle structure. On the upper left is reported a picture relative to multi-lamellar DDAB vesicles (in red/cyan colors, to distinguish the different layers), on the upper right the one related to bi-layered SDS/CTAB vesicles (in blue color). Sizes scale with the average hydrodynamic vesicle radius, inferred from DLS. In the bottom is indicated a cartoon of ABOP nano-particles with surface-bound LYS molecules. As before, regions in red indicate the dominance of positive charges (around the protein), when the blue color of the corona indicates an excess of negative charges.

The above approach helps determining the kinetic features of interactions between different *LYS-ABOP* particles. It will also be used to account for the interactions taking place between vesicles and *LYS-ABOP*. It is expected that attractions are experienced in the interaction between *LYS-ABOP* and cat-anionic vesicles (bearing a negative charge), and repulsions in the other case, *Figure 4*.

DLS alone does not allow to asses any firm statement on lysozyme binding, since the sizes of functionalized *NP*s is only slightly higher than before the reaction. That's why combination of optical absorbance with *DLS*, *CD* and electro-phoretic mobility is helpful.

The former method quantifies the amount of *ABOP*-bound protein (in native or denatured state) and whether binding is effective. The second gives information on the conformational

state of *LYS*. Electro-phoretic mobility, finally, indicates an effective surface modification of silica upon protein binding. Binding will reduce in modulus the ζ-potential values, as observed.

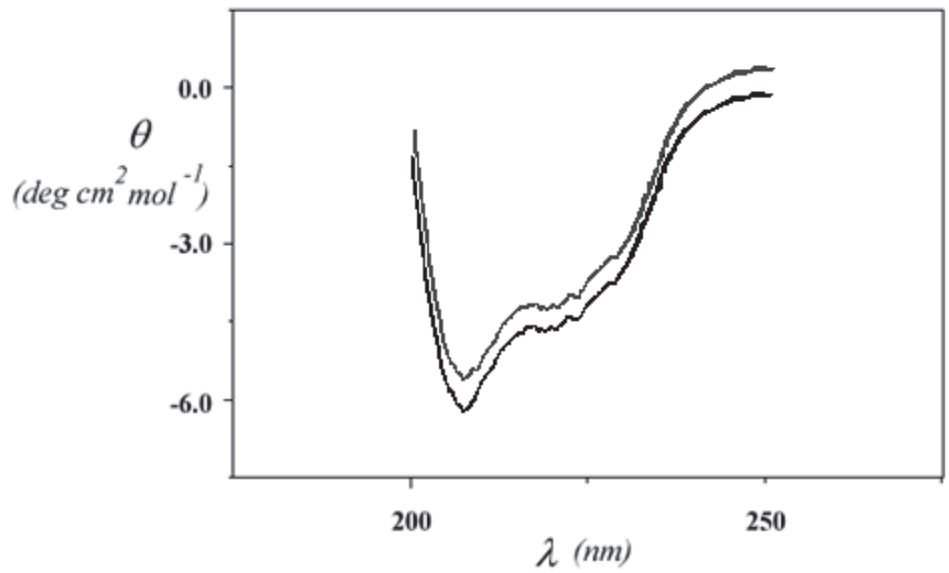

Fig. 5. CD spectrum, in molal ellipticity (θ, in deg cm^2 mol^{-1}) vs. the measuring wavelength (λ, in nm) of LYS-ABOP nano-particles, in grey color, compared to the corresponding value for bulk LYS, in black. The signal intensities were rescaled to allow for a comparison. In both cases data refer to pH 8.5, with 50.0 mmol Borax buffer, and 25.0° C. The former was upward shifted, to avoid overlapping.

Optical absorbance, performed in the 220-230 nm range, determined the presence and number of *LYS* molecules bound onto *ABOP* particles. The average value is <5±1> molecules. The uncertainty is high since the number of *NP*s in the medium is low, and scattering effects reduce the datum quality. *CD* data, *Figure 5*, indicate that the conformation of covalently bound protein is very close to its native form. Thus, the presence of bound protein was inferred by optical absorbance (and elemental analysis, as well), whereas a conformation close to the native one was inferred by *CD*.

Finally, the ζ-potential of *LYS-ABOP* particles decreases from -36 mV of the bare ones to -20, in case of protein-bound entities. Data indicate a significant *LYS* binding and surface modification, but a significant reduction of surface charge density compared to the native particles. This is because some *COOH* units are linked with *LYS* and the charge density of the particle as a whole is substantially reduced. The reduction in ζ-potential also explains why *LYS-ABOP* adducts are less kinetically stable compared to bare *ABOP*.

The optimal conditions leading to stabilization are fulfilled for *pH* values between 7.0 and 8.5. Below *pH* 7.0 the particles sizes increase significantly and such conditions were avoided. Substantial amounts of salt must be used to stabilize the dispersions in such *pH* conditions.

A scheme representing all particles considered here is in *Figure 4*. There is indicated the structure of vesicles and *LYS-ABOP* complexes, with charge distribution in evidence. It is expected that the charge distribution is responsible for interactions with both negatively or

positively charged vesicles. It is expected that the kinetic features inherent to vesicle-*LYS-ABOP* particles interactions should behave accordingly.

The analysis of kinetic data, performed by *DLS* methods, is essentially based on the supposed dominance of electrostatic interactions between particles. Were this hypothesis absolutely unrealistic, different kinetic approaches should be considered. For instance the elecctro-phoretic term in the flux equation should be critically reconsidered. Very presumably, however, binding is due to the combined effect of dominant electrostatic contributions plus hydrophobic and ancillary (osmotic?) ones into an as yet undefined mechanism.

Kinetic features. Processes related to vesicles-*NPs* interactions are dealt with in this part. Dispersions of *DDAB* and (*SDS-CTAB*), at the same nominal concentration in lipid, were mixed with tiny amounts of *LYS-ABOP* particles. The number ratio between the latter and vesicles is moderate. This allows measuring the kinetic features inherent to the interactions between *LYS-ABOP NP*s and vesicles. An eye-view to the results, *Figure 6* and *Figure 7*, indicates that the interactive processes can be rationalized on volume fraction statistics. The kinetic pathways scale with the *VES-NP* number ratio. Vesicles sizes are different each from the other, but are reasonably close to *NP*s. That means that changes in size of the scattering entities are mostly due to vesicles-*NPs* adducts. The respective kinetic pathways and the size of particles obtained at the end of the respective reactive processes are different in the two cases. In the [*DDAB*+(*LYS-ABOP*)] system sizes at equilibrium are lower compared to the [(*SDS-CTAB*)+(*LYS-ABOP*)] one. These effects are a sound indication of clustering between

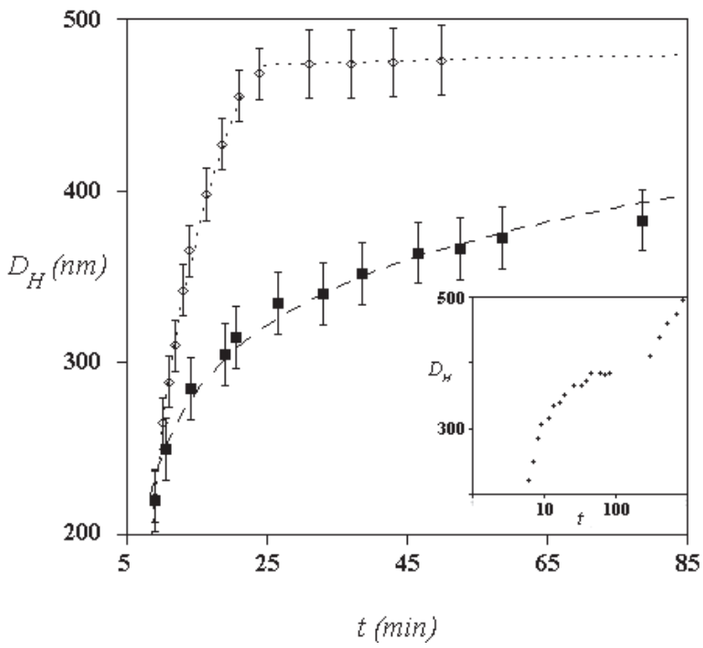

Fig. 6. Kinetics of vesicle-NP interaction inferred from DLS plots of average particles size, D_H, as a function of measuring time, t (min), for two different vesicles to LYS-ABOP nano-particles number ratios. Data refer to systems buffered with 50 mmol Borax, at 25°C. Black symbols refer to a number ratio between NP's and cat-anionic SDS-CTAB vesicles (having mole ratio between the two of 1.7/1.0) equal to 1/60 and 1/150 in the other case. In the inset is reported the long term behavior observed in the former system.

objects similar in size, driven by electrostatic interactions between the two entities. Differences in the size of super-colloids formed in these mixtures are the consequences of the interaction mechanisms and result in significant changes in size and shape (presumably) of the resulting entities. Similar features were observed in the [*DDAB*+(*LYS-ABOP*)] system, *Figure 7*. There a marked tendency to sedimentation is observed after the interactions took place. Presumably, part of the observed decrease in size may be due to sedimentation processes, occurring at the early stages of the process.

The interactions between *DDAB* and *LYS-ABOP NP*'s show a different kinetic behavior compared to the former system, with a significant increase in size at low times, followed by a substantial decrease at long ones. This behavior is controlled by the net charge of the reacting objects and indicates that electrostatic terms are significant. According to *Figure 7*, there is a pronounced redistribution of particles sizes after about 40 minutes. Such features are, very presumably, related to a structural rearrangement and eventual rupture of vesicle-*NP* adducts with time.

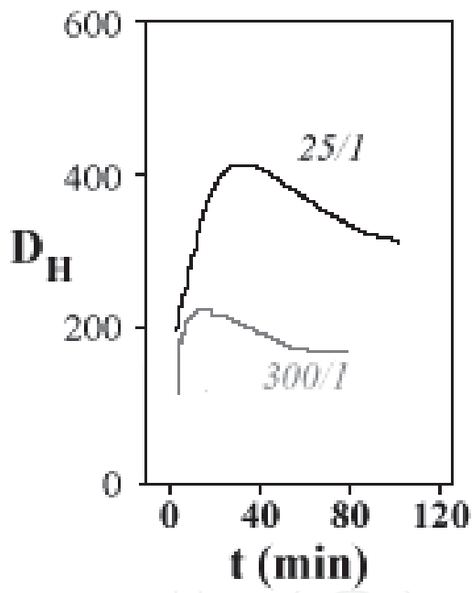

Fig. 7. Plot of the average vesicle/Lys-ABOP adducts size (in nm) with time, in minutes, upon interaction between DDAB vesicles and LYS-ABOP nano-particles. The nominal number ratio between the colloidal objects is indicated in the figure. Experimental conditions refer to the same pH and temperature values reported above.

It is also possible that adducts sedimentation takes place after some time. In words, the formation of composites colloids implies a progressive saturation mechanism in case of *SDS-CTAB* vesicles. Conversely, a significantly different behavior occurs in the *DDAB* containing system. This is put in evidence by the macroscopic appearance of the super-colloid entities formed in this way. In some instances sediments are found at the bottom of vials, in others large floating particles are observed in the medium. That means that the super-colloids formed upon interaction between vesicles and nano-particles differ each from the other in packing density and surface charge, to mind but a few effects.

According to *Figure 8*, for instance, it is evident that entities made of *DDAB* and *LYS-ABOP* particles do form small aggregates, held together by significant forces, presumably electrostatic in nature. According to optical microscopy, it results that these composite objects are made of different sub-domains, differing each from the other in optical appearance and color. Apparently, there is no significant relation between the average stoichiometry of adducts made by vesicles and nano-particles and that pertinent to mother solution. In words, there is no direct proportionality between number of particles in the medium and composition of the precipitates.

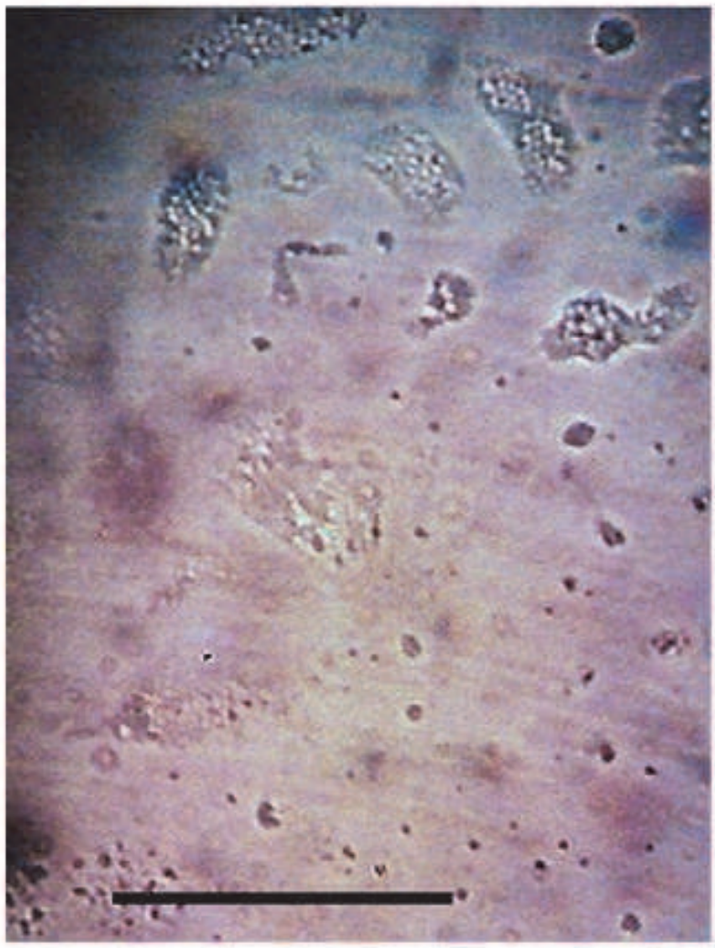

Fig. 8. Vesicle- PFNP clusters, obtained by mixing DDAB and PFNP in number ratios 300/1 and recovering the precipitates. They are visualized through a Zeiss Optical Microscope using normal light. The bar size in the bottom is 100 μm large.

6. Conclusions

The results reported here indicate the possibility to get "*hybrid*" colloid composites from the interactions between *LYS-NPs* complexes and vesicles. The reported results refer to the phenomenological aspects of the interaction process, as it was inferred from *DLS*. Very

presumably, the observed features are related to structural rearrangements and to eventual rupture of vesicle-*NP* adducts with time. In one case, apparently, the sedimentation of adducts takes place after some time. In others, large floating objects are present in the dispersing medium.

Depending on the forces active between vesicles and *LYS-NPs*, it is possible that the kinetics of adducts formation follows different pathways. In the case of *SDS-CTAB* cat-anionic vesicles (bearing a substantial negative charge), the interaction mechanism obeys a pseudo first-order mechanism, controlled by the number ratio between the components. In the interaction between *DDAB* vesicles and *LYS-NPs*, conversely, the situation is more cumbersome to be rationalized. In this latter case, it is presumed that the interaction mechanism implies the formation of a transient state (characterized by a maximum in *DLS* plots); after some time the mixed colloid particles rearrange and change in size and shape. It is also possible that the large increase in size observed in this system is due to the incipient nucleation of particles, which precipitate after some time.

Some questions are still under debate on the biological implications of the above systems. However, when *LYS-ABOP* particles interact with cells, it is expected that the reactive behavior (mostly the one relative to surface adsorption) will be close to that reported in case of cat-anionic surfactant mixtures. In fact, cells are negatively charged and are generally composed by mixtures of oppositely charged lipids. On this regard, thus, cat-anionic systems are much more effective as bio-mimetic models compared to other currently used lipid dispersions. It must be also considered that the mechanisms controlling the pynocytosis of particles adsorbed onto cells require the deformation of the latter. In fact, vesicles made by different lipids are more prone to be deformed and envaginate [25], as a consequence of local changes in composition associated to adsorption of charged and bulky entities onto them. This implies the migration of the lipid components in the bi-layer and induces a local deformation of vesicles, making possible particles uptake into cells. More dedicated investigation is required to clarify such aspects.

Another relevant question deals with use of the above systems in modeling bio-mimetic processes. In nature there are cases of interactions between "*hard*" and "*soft*" particles, as, for instance, in the interactions between viruses and other viral vectors and cells [26,27]. From such a point of view, the ones presented here are excellent mimetic models of the above interactions, because viruses are generally covered with enzymes attaching onto the surface of cells and tissues. Preparing nano-particles sharing some properties in common to viruses (having, for instance, a similar surface coverage) would help understanding the physical grounds underlying the interactions between viruses and cells.

7. Acknowledgments

This work was made possible through a financial support from La Sapienza University. F.D.P. wishes to acknowledge the Ministry of Education for financing her stay in Barcelona, where she completed the characterization of the above mixtures.

Financial support from MICIN CTQ2010-14897, Generalitat de Catalunya, through the 2009SGR1331 grant and COST Action Project on Chemistry at Interfaces, D36, are gratefully acknowledged.

Thanks to A. Scipioni, Dept. of Chemistry at La Sapienza, for help in performing *CD* spectra, and for fruitful discussions on some aspects of the manuscript. Thanks also to G. Risuleo,

Dept. of Molecular Biology at La Sapienza, for suggestions on the biological implications of these systems.

8. References

[1] F. Feng, F. Le, L. An, S. Wang, Y. Li, D. Zhu, *Adv. Mater.*, 2008, *20*, 2959.
[2] H.K. Valo; P.H. Laaksonen; L.J. Peltonen; M.B. Linder; J.T. Hirvonen; T.J. Laaksonen, *ACS Nano*, 2010, *4*, 1750.
[3] C. Mateo; J.M. Palomo; G. Fernàndez-Lorente; J.M. Guisàn; R. Fernàndez-Lafuente, *Enzyme Microbial Technol.*, 2007, *40*, 1451.
[4] J.L. Brash; T.A. Horbett, *ACS Symp. Ser.* (*Proteins at Interfaces*), 1995, Vol. *602*, p. 1.
[5] E. Soussan; S. Cassel; M. Blanzat; I. Rico-Lattes, *Angew. Chem. Int. Ed.*, 2009, *48*, 274.
[6] C. Letizia, P. Andreozzi, A. Scipioni, C. La Mesa, A. Bonincontro, E. Spigone, *J. Phys. Chem. B*, 2007, *111*, 898.
[7] J. Szebeni; L. Baranyi; S. Savay; J. Milosevits; R. Bunger; P. Laverman; J.M. Metselaar; G. Storm; A. Chanan-Khan; L. Liebes; F.M. Muggia; R. Cohen; Y. Barenholz; C.R. Alving, *J. Liposome Res.*, 2002, *12*, 165.
[8] D. Simberg; S. Weisman; Y. Talmon; Y. Barenholz, *Crit. Rev. Ther. Drug Carrier Syst.*, 2004, *21*, 257.
[9] H.T. Jung; B. Coldren; J.A. Zasadzinski,; D.J. Iampietro; E.W. Kaler, *Proc. Nat. Acad. Sci. U.S.A.*, 2001, *98*, 1353.
[10] E.F. Marques; O. Regev; A. Khan; B. Lindman, *Adv. Colloid Interface Sci.*, 2003, *100-102*, 83.
[11] A. Bonincontro; E. Spigone; M. Ruiz Peña; C. Letizia; C. La Mesa, *J. Colloid Interface Sci.*, 2006, *304*, 342.
[12] A. Bonincontro; C. La Mesa; C. Proietti; G. Risuleo, *Biomacromolecules*, 2007, 8, 1824.
[13] C. Aiello; P. Andreozzi; C. La Mesa; G. Risuleo, *Colloids Surf. B: Biointerfaces*, 2010, *78*, 149.
[14] T.H. Galow; K. Boal; V.M. Rotello, *Adv. Mater.*, 2000, *12*, 576.
[15] A. Zielenciewicz, *J. Therm. Anal. Calor.* 2001, *65*, 467.
[16] K. Monkos, *Biochim. Biophys. Acta: Prot. Struct. Mol. Enzymol.*, 1997, *1339*, 304.
[17] G. Gente; A. Iovino; C. La Mesa, *J. Colloid Interface Sci.*, 2004, *274*, 458.
[18] A. Budhian; S.J. Siegel; K.I. Winey, *Intern. J. Pharmaceutics*, 2007, *336*, 367.
[19] F. De Persiis; P. Andreozzi; C. La Mesa; R. Pons, *submitted*.
[20] P. Andreozzi; S.S. Funari; C. La Mesa; P. Mariani; M.G. Ortore; R. Sinibaldi; F. Spinozzi, *J. Phys. Chem. B*, 2010, *114*, 8056.
[21] P. Andreozzi; A. Bonincontro; C. La Mesa, *J. Phys. Chem. B*, 2008, *112*, 3339.
[22] S. W. Provencher, *Comput. Phys. Comm.* 1982, *27*, 213.
[23] A.W. Adamson, *Physical Chemistry of Surfaces*, 5th ed.; Wiley & Sons: New York, 1990; Chapt. *V*, p. 203.
[24] J.B. Berne; R. Pecora, *Dynamic Light Scattering*; Wiley & Sons: New York, 1976; Chapt. *VI*, p. 96.
[25] D. Fennel Evans; H. Wennerstroem, *The Colloidal Domain: where Physics, Chemistry, Biology and Technology meet*, VCH Publishers, Inc.; New York, 1994, *Chapt. VI*, p. 239.
[26] M.F. Hagan, *J. Chem. Phys.*, 2009, *130*, 114902/1.

[27] X. Huang; L.M. Bronstein; J. Retrum; C. Dufort; I. Tsvetkova; S. Aniagyei; B. Stein; G. Stucky; M. McKenna; N. Remmes; D. Baxter; C.C. Kao; B. Dragnea, *Nano Lett.*, 2007, *7*, 2407.

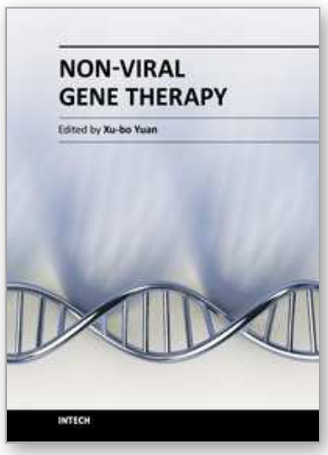

Non-Viral Gene Therapy

Edited by Prof. Xubo Yuan

ISBN 978-953-307-538-9
Hard cover, 696 pages
Publisher InTech
Published online 07, November, 2011
Published in print edition November, 2011

This book focuses on recent advancement of gene delivery systems research. With the multidisciplinary contribution in gene delivery, the book covers several aspects in the gene therapy development: various gene delivery systems, methods to enhance delivery, materials with modification and multifunction for the tumor or tissue targeting. This book will help molecular biologists gain a basic knowledge of gene delivery vehicles, while drug delivery scientist will better understand DNA, molecular biology, and DNA manipulation.

INTECH
open science | open minds

InTech Europe
University Campus STeP Ri
Slavka Krautzeka 83/A
51000 Rijeka, Croatia
Phone: +385 (51) 770 447
Fax: +385 (51) 686 166
www.intechopen.com

InTech China
Unit 405, Office Block, Hotel Equatorial Shanghai
No.65, Yan An Road (West), Shanghai, 200040, China
中国上海市延安西路65号上海国际贵都大饭店办公楼405单元
Phone: +86-21-62489820
Fax: +86-21-62489821

IntechOpen